OSIRIS

Optical, Spectroscopic, and Infrared Remote Imaging System

Determination of the absolute calibration coefficients to radiometrically calibrate OSIRIS images

RO-RIS-MPAE-TN-074

Issue: 2

Revision: a

30 November 2021

Prepared by:

Carsten Güttler

Approval Sheet

Digitally signed by Carsten Güttler
Date: 2021.12.20 14:30:05 +01'00'

prepared by: Carsten Güttler (signature/date)

Digitally signed by
Holger Sierks
Date: 2021.12.20
15:40:28 +01'00'

approved by: Holger Sierks (signature/date)

Document Change Record

Iss./Rev.	Date / Author	Pages affected	Description
D / -	5 May 2015 C. Tubiana	all	first draft
1 / -	18 Jun 2015 C. Tubiana	all	first issue
1 / a	22 Feb 2017 C. Tubiana	Sect. 4	added Sect. 4
1 / b	6 Feb 2018 C. Tubiana	Sect. 2 and 3	- added Sect. 3 - clarified text and equation in Sect. 2
2 / -	17 Nov 2021 C. Güttler	all	- full re-write of Sect. 2 with new abs-cal factors - new solar and Vega spectra (Sect. 3.1.2)
2 / a	30 Nov 2011 C. Güttler	Sect. 2.3	- added abs-cal factor for WAC11 - reference on pinhole affected filters

Table of contents

1 General aspects 1
1.1 Scope 1
1.2 Introduction 1
1.3 Reference Documents 1
1.4 Acronyms and Abbreviations 1
2 Determination of Absolute Calibration Factors 3
2.1 Sensitivity and Star Spectra 3
2.2 Vega Aperture 4
2.3 Absolute Calibration Factors 6
2.4 Validation 9
3 Camera Throughput and Spectra of Stars 11
3.1.1 Instrument Throughput 11
3.1.2 Spectral Irradiance of Sun and Calibration Stars 13
4 Calibration files used by OsiCalliope 15

List of Figures

Figure 1: Aperture signal per filter compared to signals in 2014 (version 1/b of this document). . 6
Figure 2: Reflectance factor per filter compared to factors from 2014 (version 1/b of this document). 9
Figure 3: Spectral irradiance of 16 Cyg determined from aperture photometry in comparison to scaled solar spectrum. 10
Figure 4: Reflectance of 4 Vesta compared to OSIRIS photometry with new reflectance factors 10
Figure 5: Measured total reflectivity of the mirrors and transmissivity of the ARPs for NAC (left) and WAC (right). 11
Figure 6: Quantum efficiency by design of the OSIRIS CCDs. 12
Figure 7: Quantum efficiency of the NAC (left) and of the WAC (right) CCD, as measured on the flight models at room temperature (295 K) and close to operational temperature (180 K). . 12

List of Tables

Table 1: Camera parameters (constants). Derived values are rounded to three significant digits. . 4

Table 2: Pinhole affected filters. 7

Table 3: Derived abs-cal factors and required integrals to compute these. Values marked with (*) are based on 16 Cyg, all others are based on Vega. Filters marked by (**) have theoretical calibration factors from Eq. 9. 8

Table 4: Quantum efficiency of the NAC and of the WAC CCD, as measured on the flight models at room temperature (295 K) and close to operational temperature (180 K). 13

Table 5: Spectral energy distributions. 14

1 General aspects

1.1 Scope

This document describes how the absolute calibration coefficients to radiometrically calibrate OSIRIS images are determined.

1.2 Introduction

The absolute calibration factors are used for a step of the OSIRIS calibration pipeline [RD6], where an image in DN s^{-1} units is multiplied with an abs-cal factor to convert it to spectral radiance in W m^{-2} sr^{-1} nm^{-1}.

This document describes absolute calibration factors determined over the full mission in 2021, whereas previous versions of this document describe calibration factors determined from a Vega calibration sequence in May 2014.

1.3 Reference Documents

no.	document name	document number, Iss./Rev.
RD1	Operations User Manual	RO-RIS-MPAE-MA-004, D/s
RD2	Pre-calibration report CCD #242 (WAC FM)	RO-RIS-MPAE-RP-073, 1/-
RD3	NAC CCD # 243 Acceptance Test Report	RO-RIS-MPAE-RP-355, 1/-
RD4	measured_13_03_01.txt (V. Da Deppo, personal communication)	
RD5	Misura spettrofotometrica del trattamento ottico riflettate del 2° lotto di produzione M1-M2.	OS-GAL-TN-2001 2/0
RD6	OSIRIS calibration pipeline OsiCalliope	RO-RIS-MPAE-MA-007
RD7	OSIRIS camera distortion and boresight correction	RO-RIS-MPAE-TN-081
RD8	Acquisition and processing of flat field images for OSIRIS calibration	RO-RIS-MPAE-TN-075
RD9	Refinement of Absolute Calibration Factors	RO-RIS-MPAE-TN-095
RD10	NAC and WAC Optical Band-pass Filter transmissions	RO-RIS-MPAE-TN-091, 1/b
RD11	Implications of Transmission Measurements of Optical Elements	RO-RIS-MPAE-RP-361, 1/a
RD12	Assessment of OSIRIS Filter Pinholes	RO-RIS-MPAE-RP-362

1.4 Acronyms and Abbreviations

CCD	Charge-Coupled Device
DN	Digital Numbers (or counts)
GRM	Ground Reference Model
IAU	International Astronomical Union

iFoV	Instantaneous field of view
MPS	Max Planck Institute for Solar System Research
OSIRIS	Optical, Spectroscopic, and Infrared Remote Imaging System
PTB	Physikalisch Technische Bundesanstalt
QE	Quantum Efficiency
TSI	Total Solar Irradiance

2 Determination of Absolute Calibration Factors

The absolute calibration factor f_{abs} to convert OSIRIS images in DN s^{-1} to spectral radiance units (W m^{-2} sr^{-1} nm^{-1}) is determined by the ratio of the measured signal of a star R_{star} and its flux at the centre wavelength $\langle E_{\mathrm{star}} \rangle$, multiplied with the pixel size (square iFoV) k:

$$f_{\mathrm{abs}} = k \cdot \frac{R_{\mathrm{star}}}{\langle E_{\mathrm{star}} \rangle} \qquad \text{Eq. 1}$$

The pixel size is a constant per camera, which follows from the physical pixel size and the camera focal length after distortion correction, to which the images will be corrected in the determination of R_{star} (see Sect. 2.2). Camera constants are provided in Table 1.

In contrast to earlier versions of this document (before 2/-), we define the centre wavelength as the sensitivity-weighted centroid wavelength

$$\langle \lambda \rangle = \frac{\int \lambda \cdot S(\lambda)\, d\lambda}{\int S(\lambda)\, d\lambda} \qquad \text{Eq. 2}$$

and the centre-wavelength flux of a star accordingly as the sensitivity-weighted flux

$$\langle E_{\mathrm{star}} \rangle = \frac{\int E_{\mathrm{star}}(\lambda) \cdot S(\lambda)\, d\lambda}{\int S(\lambda)\, d\lambda} \quad . \qquad \text{Eq. 3}$$

Here, λ is the wavelength, $E_{\mathrm{star}}(\lambda)$ is the spectral irradiance of a star, and

$$S(\lambda) = \frac{A \cdot T(\lambda) \cdot Q(\lambda) \cdot \lambda}{G \cdot h \cdot c} \qquad \text{Eq. 4}$$

is the camera sensitivity function. The required parameters to determine the sensitivity function are camera aperture area A, the camera transmissivity $T(\lambda)$ (per filter; including mirrors, filters and ARP), the CCD quantum efficiency $Q(\lambda)$ in electrons per photons, and the camera electronic gain G. The physical constants c and h are the speed of light and the Planck constant, respectively.

In this definitions, with precise knowledge of all given parameters, the expected signal of a star can be written as

$$\tilde{R}_{\mathrm{star}} = \int E_{\mathrm{star}}(\lambda) \cdot S(\lambda)\, d\lambda \quad . \qquad \text{Eq. 5}$$

For the precise determination of the absolute calibration factors however, one uses the measured signal of a star R_{star}, and for consistency with earlier versions of this document we use

$$f_{\mathrm{abs}} = k \cdot \frac{R_{\mathrm{star}}}{\langle E_{\mathrm{Sun}} \rangle} \cdot \frac{\int E_{\mathrm{Sun}}(\lambda) \cdot S(\lambda)\, d\lambda}{\int E_{\mathrm{star}}(\lambda) \cdot S(\lambda)\, d\lambda} \,, \qquad \text{Eq. 6}$$

which can be shown to be identical to Eq. 1 with the use of Eq. 3.

The calibrator for OSIRIS, indicated by the index 'star', is mostly Vega. For those filters where Vega images are not acquired or not usable, the star is 16 Cyg (A&B).

2.1 Sensitivity and Star Spectra

For the computation of the absolute calibration factor in Eq. 6, it is fundamental to precisely determine two integrals $\tilde{R}_{\mathrm{star}}$ from Eq. 5 and $\langle E_{\mathrm{Sun}} \rangle$ from Eq. 3. The index 'star' can be Vega,

16 Cyg, or Sun, the utilised spectral irradiance $E_{\mathrm{star}}(\lambda)$ of these three objects are described in Sect. 3.

The sensitivity function $S(\lambda)$ depends on camera and filter combination. The aperture area A (derived from focal length and F-number) and the gain G are listed in Table 1. The throughput $T(\lambda)$ is the product of the two filter transmission curves (combination of filter and focus plate for NAC, one filter for WAC), the ARP transmission curve, and the mirror reflectance curve. Details of these are discussed in Sect. 3. The quantum efficiency $Q(\lambda)$ is given in photons per electron and therefore requires a conversion to energy ratio by the factor λ/hc. It is also discussed in Sect. 3.

Table 1: Camera parameters (constants). Derived values are rounded to three significant digits.

Parameter	NAC	WAC	Reference
Physical pixel size	$13.5 \times 13.5\ \mu\mathrm{m}^2$	$13.5 \times 13.5\ \mu\mathrm{m}^2$	[RD1]
F-number	8.0	5.6	[RD1]
Focal length	717.322 mm	135.68 mm	[RD7]
Gain	$3.1\ \mathrm{e}^-\ \mathrm{DN}^{-1}$	$3.1\ \mathrm{e}^-\ \mathrm{DN}^{-1}$	[RD6]
Pixel size (square iFoV)	$3.54 \cdot 10^{-10}$ sr	$9.90 \cdot 10^{-9}$ sr	derived
Aperture area	$63.1\ \mathrm{cm}^2$	$4.61\ \mathrm{cm}^2$	derived

For the numerical integration of the curve, the wavelength dependent factors of the sensitivity curve $S(\lambda)$ are resampled on a 0.1 nm resolution by linear interpolation and multiplied. In contrast to earlier calculations, the resulting sensitivity curve is not cropped for the band pass but instead integrated over the full range of non-zero quantum efficiency. The sensitivity curve multiplied with the integrator of choice (wavelength or resampled irradiance) is then integrated with a 5-point Newton Coates integration (Boole's rule).

The results for $\langle\lambda\rangle$, $\langle E_{\mathrm{Sun}}\rangle$, $\tilde{R}_{\mathrm{Sun}}$ and $\tilde{R}_{\mathrm{star}}$ (with 'star' denoting Vega or 16 Cyg in this case) are listed in Table 3.

2.2 Vega Aperture

The measured star signal R_{star} in Eq. 6 is in DN s^{-1} and based on aperture photometry of a calibrator star. The calibrator for OSIRIS is Vega wherever possible and the 16 Cyg system if no adequate Vega data is available.

The aperture algorithm is adapted to OSIRIS Vega observations and can be outlined as follows:

1. Read calibrated level 2 (CODMAC L3) OSIRIS image and multiply with absolute calibration factor used for this specific image and listed in the image header HISTORY section.
2. Correct pixel size per pixel by multiplying with the relative pixel size map (see [RD7] for details).
3. Convert spectral flatfield correction from Sun to Vega by multiplying the image with the Sun spectral flatfield and dividing by the Vega spectral flatfield (only Vega, not for 16 Cyg; see [RD8] for details).

4. Find star and crop a 101×101 pixel area around star's brightest pixel (defined as centre).
5. Filter out cosmics in the background and the outer aperture area (radius > 10 for Vega; see [RD9] for details).
6. Apply vertical equalisation of line dependant readout offset (software windowed images only; see [RD9] for details).
7. Compute background as arithmetic mean of the background region (radius ≥ 25 to < 50 for Vega) and subtract value from image.
8. Compute aperture signal as plain sum of all pixels in the aperture region (radius < 25 for Vega).

The choice of a plain mean and sum in steps 7 and 8 in contrast to commonly used filtering methods (median for example) is based on the following rationale: Vega is bright such that there are no visible background stars for the selected exposure times. The image shows small noise speckles in the background as well as in the aperture area. If these were filtered out in the background area, they would count as additional signal in the aperture area. In contrast to that, with the assumption of an even spatial distribution of the noise pattern, a plain average in step 7 corrects for the pattern in the aperture region.

The error of the aperture signal S can be written as

$$\Delta S = \sqrt{N{\sigma_B}^2 + \left(\frac{N \cdot \sigma_B}{\sqrt{M}}\right)^2 + \sum_{i=1}^{N} \frac{s_i}{t_{\mathrm{exp}} \cdot G}}\ , \qquad \text{Eq. 7}$$

where N and M are the number of pixels in the aperture and background area, respectively, σ_B is the standard deviation of the background measurement, s_i is the signal (in DN s^{-1}) of a pixel with index i, t_{exp} is the mean effective exposure time of the image, and G is the gain. The three components of the equation are the contributions from the random noise, the error of the background determination, and the shot noise. The equation is derived in [RD9].

The star signal R_{star} from this method is computed for all possible Vega images with the following selection criteria: no shutter error, amplifier B, no NAC images before 2010, no overexposed pixel in the aperture or background region, and no unfiltered cosmics (each image was visually checked for this purpose). This results in 563 images that could be analysed.

For NAC filter combinations 21, 31, and 34, no adequate Vega images were available, such that the same procedure (with adapted parametrisation in terms of aperture size) was applied to the 16 Cyg system by integrating over both stars (formally three stars but only two are visible with OSIRIS). The centre for integration in that case is the brightness peak of a highly blurred image, which resulted in a reliable centre between the two stars.

The signals were averaged per filter combination with a weighted mean using the individual measurement errors ΔS. To assess the resulting error, we compared the propagated standard error from the individual errors with the standard error of the subset. The plain standard error was typically a small factor (≈ 1.5) larger than the propagated error, which indicates an unaccounted source of error but nonetheless argues for plausibility. The factor is substantially larger (up to 4) for pinhole affected filters. For filter combinations with few images, the standard error is smaller than the propagated error. We use the maximum of the two errors as the measurement error.

The change of aperture signals with errors in comparison to aperture signals from 2014 absolute calibration factors (version 1/b of this document) is presented in Figure 1. All resulting star signals per filter combination, together with the relative errors, are listed in Table 3.

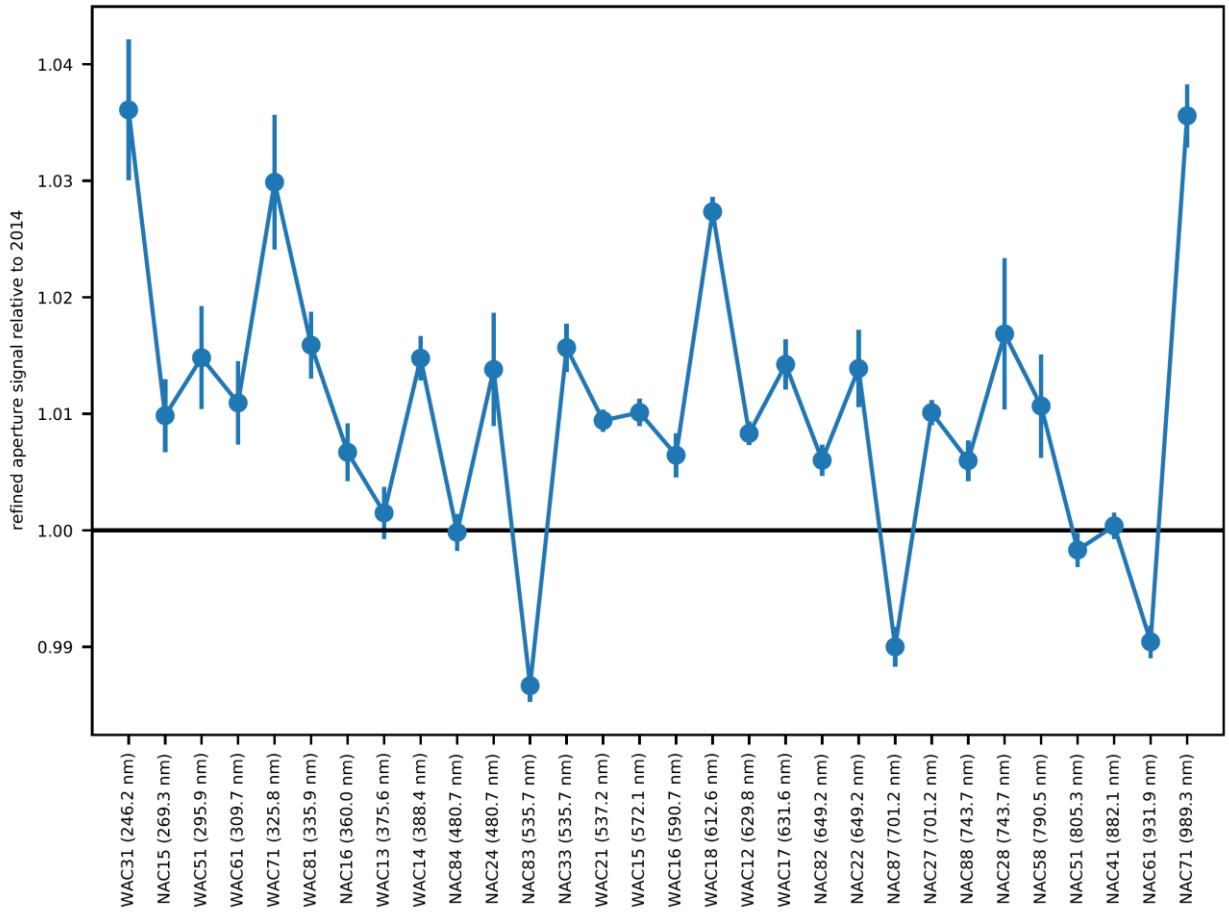

Figure 1: Aperture signal per filter compared to signals in 2014 (version 1/b of this document).

2.3 Absolute Calibration Factors

Star aperture signal from Sect. 2.2 and flux integrals from Sect. 2.1 are compiled in Table 3. Using Eq. 6, we can derive the absolute calibration factors f_{abs} per filter combination. As mentioned above, this is equivalent with using Eq. 1, which means that the error of the solar spectrum does not contribute to the absolute calibration factors, as it formally cancels out. The error Δf_{abs} therefore is given as

$$\frac{\Delta f_{\mathrm{abs}}}{f_{\mathrm{abs}}} = \sqrt{\left(\frac{\Delta R_{\mathrm{star}}}{R_{\mathrm{star}}}\right)^2 + \left(\frac{\Delta \langle E_{\mathrm{star}} \rangle}{\langle E_{\mathrm{star}} \rangle}\right)^2} \quad , \qquad \text{Eq. 8}$$

with the second term, the error of the star spectrum, being 1% for Vega and 2.5% for 16 Cyg.

Since no star observations are available for WAC filter 11 (empty), this can only be computed as a theoretical value. Applying Eq. 1 for the Sun and approximating R_{Sun} as $\tilde{R}_{\mathrm{Sun}}$, we get

$$f_{\mathrm{abs}} = k \cdot \frac{\int E_{\mathrm{Sun}}(\lambda) \cdot S(\lambda)\, d\lambda}{\langle E_{\mathrm{Sun}} \rangle} = k \cdot \int S(\lambda)\, d\lambda \qquad \text{Eq. 9}$$

This equation can be solved from the knowledge of the instrument but with a larger uncertainty. For the two broadband visible filters Red (F12) and Green (F21), Table 3 shows that $R_{\mathrm{Vega}}/\tilde{R}_{\mathrm{Vega}}$ is 1.16, i.e., the observed flux is 16% higher than the theoretical value. In terms of total flux, these two represent $\sim 50\%$ of the energy in filter 11. We therefore apply this correction to the calibration factor for filter 11 after solving Eq. 9, and provide the value in Table 3. In this case, the resulting error is significantly larger and can only be estimated. We assume an error of 20%, which is in the order of the applied correction.

For a comparison of the absolute calibration factors with respect to calibration factors used earlier, we present the reflectance factor $f_{\mathrm{abs}} \cdot \langle E_{\mathrm{Sun}} \rangle$, which is the factor to which images in reflectance units will change. This is presented in Figure 2. Changes are within 3% for most NAC filters and for visible WAC filters.

NAC filters 21, 31, 34, and 81 have a larger variation but those were not updated in 2014. 16 Cyg aperture photometry applying 2014 calibration factors showed a large deviation with respect to the 16 Cyg spectrum such that these 2014 factors must be considered doubtful before this update.

WAC filters UV245 (F31) and CS (F41) in the UV range also have a larger deviation in the 2014 calibration due to the unaccounted signal from out-of-band transmission.

It must be noted that a number of UV filters are affected by out-of-band leakage due to pinholes, i.e., physical holes in the filters' band-pass coating [RD12]. This was observed by microscope images of flight and spare-filter surfaces as well as spectral transmission measurements at different locations on these. The transmission measurements show an elevated transmission for wavelengths above 400 nm. The strength of leakage on the spare filters depends on the location on the filter, as well as on the filter age (getting stronger over time). The source of the pinholes is understood to be a reaction of fluorine and humidity embedded in the aluminium layers and further humidity throughout storage once a pinhole is created. The storage of the reference filters plays a dominant role, such that spare filters cannot be considered as representative but only indicative. The affected filters are listed in Table 2. The photometric accuracy of the clearly pinhole affected flight filters can be off by up to a factor 2, so these filters have to be used with care.

Table 2: Pinhole affected filters.

Filter Name	No.	Assessment
WAC UV-245	F31	clearly affected: visible in photographs, transmission, flat fields
WAC CS	F41	clearly affected: visible in photographs, transmission, flat fields
WAC UV-295	F51	mildly affected: visible in flat field, weak and localised
WAC OH	F61	mildly affected: visible in flat field, localised
WAC UV-325	F71	strongly affected: visible in photographs, transmission, flat fields
WAC NH	F81	mildly affected: visible in flat field, localised
NAC FUV	F15	likely not affected: spare filters affected mildly after storage

Table 3: Derived abs-cal factors and required integrals to compute these. Values marked with (*) are based on 16 Cyg, all others are based on Vega. Filters marked by (**) have theoretical calibration factors from Eq. 9.

camera	filter	$\langle\lambda\rangle$	$\langle E_{\mathrm{Sun}}\rangle$	$\tilde{R}_{\mathrm{Sun}}$	$\tilde{R}_{\mathrm{star}}$	R_{star}	ΔR_{star}	f_{abs}	Δf_{abs}
NAC	15	265.4	1.87E-01	1.70E+15	3.51E+05	2.63E+05	0.310%	2.43E+06	1.047%
NAC	16	364.93	1.03E+00	4.54E+16	1.72E+06	1.43E+06	0.244%	1.29E+07	1.029%
NAC	21(*)	667.49	1.42E+00	2.54E+18	3.79E+05	3.62E+05	0.300%	6.06E+08	2.518%
NAC	22	648.16	1.57E+00	5.06E+17	6.92E+06	7.33E+06	0.326%	1.21E+08	1.052%
NAC	23	536.07	1.84E+00	3.31E+17	6.97E+06	7.47E+06	0.358%	6.82E+07	1.062%
NAC	24	481.76	1.96E+00	3.44E+17	9.14E+06	9.57E+06	0.478%	6.49E+07	1.108%
NAC	26	365.7	1.03E+00	4.30E+16	1.63E+06	1.33E+06	1.336%	1.20E+07	1.669%
NAC	27	699.48	1.43E+00	1.13E+17	1.35E+06	1.37E+06	0.105%	2.84E+07	1.005%
NAC	28	742.5	1.28E+00	3.08E+17	3.42E+06	3.49E+06	0.638%	8.66E+07	1.186%
NAC	31(*)	666.16	1.43E+00	2.59E+18	3.87E+05	3.72E+05	0.123%	6.16E+08	2.503%
NAC	32	648.16	1.57E+00	5.24E+17	7.17E+06	7.57E+06	0.228%	1.25E+08	1.026%
NAC	33	536.04	1.84E+00	3.43E+17	7.23E+06	7.62E+06	0.201%	6.95E+07	1.020%
NAC	34(*)	481.7	1.96E+00	3.58E+17	5.35E+04	5.44E+04	1.176%	6.57E+07	2.763%
NAC	35	293.74	3.93E-01	4.68E+14	4.36E+04	3.21E+04	2.565%	3.10E+05	2.753%
NAC	36	367.47	1.04E+00	3.74E+16	1.43E+06	1.16E+06	1.317%	1.03E+07	1.654%
NAC	37	699.47	1.43E+00	1.17E+17	1.40E+06	1.45E+06	1.069%	2.99E+07	1.464%
NAC	38	742.35	1.28E+00	3.15E+17	3.51E+06	3.57E+06	0.303%	8.84E+07	1.045%
NAC	41	880.4	9.29E-01	1.14E+17	1.07E+06	9.98E+05	0.114%	4.05E+07	1.006%
NAC	51	804.51	1.11E+00	1.00E+17	9.95E+05	9.98E+05	0.144%	3.21E+07	1.010%
NAC	58	791.24	1.14E+00	7.69E+15	7.82E+04	7.69E+04	0.438%	2.34E+06	1.092%
NAC	61	930.79	8.35E-01	4.04E+16	3.78E+05	3.24E+05	0.139%	1.47E+07	1.010%
NAC	71	985.17	7.46E-01	1.79E+16	1.60E+05	1.12E+05	0.260%	5.94E+06	1.033%
NAC	81	678.58	1.44E+00	8.06E+16	1.36E+06	1.33E+06	0.289%	1.93E+07	1.041%
NAC	82	651.64	1.56E+00	1.43E+16	1.95E+05	1.95E+05	0.130%	3.26E+06	1.008%
NAC	83	536.41	1.84E+00	9.66E+15	2.03E+05	2.02E+05	0.141%	1.85E+06	1.010%
NAC	84	480.3	1.97E+00	1.08E+16	2.89E+05	2.93E+05	0.157%	1.97E+06	1.012%
NAC	86	396.55	1.09E+00	1.64E+14	7.14E+03	6.74E+03	0.983%	5.04E+04	1.402%
NAC	87	700.49	1.43E+00	5.30E+15	6.33E+04	6.34E+04	0.169%	1.32E+06	1.014%
NAC	88	741.57	1.29E+00	1.58E+16	1.76E+05	1.75E+05	0.173%	4.32E+06	1.015%
WAC	11(**)	634.06	1.43E+00	2.01E+17	3.98E+06	n/a	n/a	1.61E+09	20.00%
WAC	12	629.66	1.63E+00	6.80E+16	1.01E+06	1.17E+06	0.099%	4.79E+08	1.005%
WAC	13	381.66	1.12E+00	5.64E+14	2.06E+04	1.89E+04	0.221%	4.60E+06	1.024%
WAC	14	406.32	1.07E+00	2.69E+14	1.61E+04	1.60E+04	0.187%	2.49E+06	1.017%
WAC	15	571.36	1.80E+00	4.01E+15	7.10E+04	8.22E+04	0.114%	2.55E+07	1.007%
WAC	16	589.45	1.73E+00	1.56E+15	2.61E+04	3.05E+04	0.187%	1.04E+07	1.017%
WAC	17	630.96	1.63E+00	1.21E+15	1.74E+04	2.05E+04	0.211%	8.62E+06	1.022%
WAC	18	611.78	1.69E+00	4.66E+15	7.12E+04	8.38E+04	0.121%	3.21E+07	1.007%
WAC	21	535.69	1.84E+00	2.43E+16	5.13E+05	5.96E+05	0.093%	1.52E+08	1.004%
WAC	31	248.46	6.52E-02	1.63E+13	9.87E+03	5.52E+03	0.582%	1.38E+06	1.157%
WAC	41	262.66	1.18E-01	1.13E+13	3.72E+03	1.83E+03	0.885%	4.68E+05	1.335%
WAC	51	297.95	5.24E-01	7.45E+13	5.25E+03	3.15E+03	0.433%	8.47E+05	1.090%
WAC	61	316.94	6.45E-01	3.36E+13	1.87E+03	1.31E+03	0.354%	3.61E+05	1.061%
WAC	71	324.81	8.62E-01	1.48E+14	5.83E+03	4.46E+03	0.559%	1.30E+06	1.146%
WAC	81	344.73	9.33E-01	5.37E+13	1.89E+03	1.45E+03	0.282%	4.38E+05	1.039%

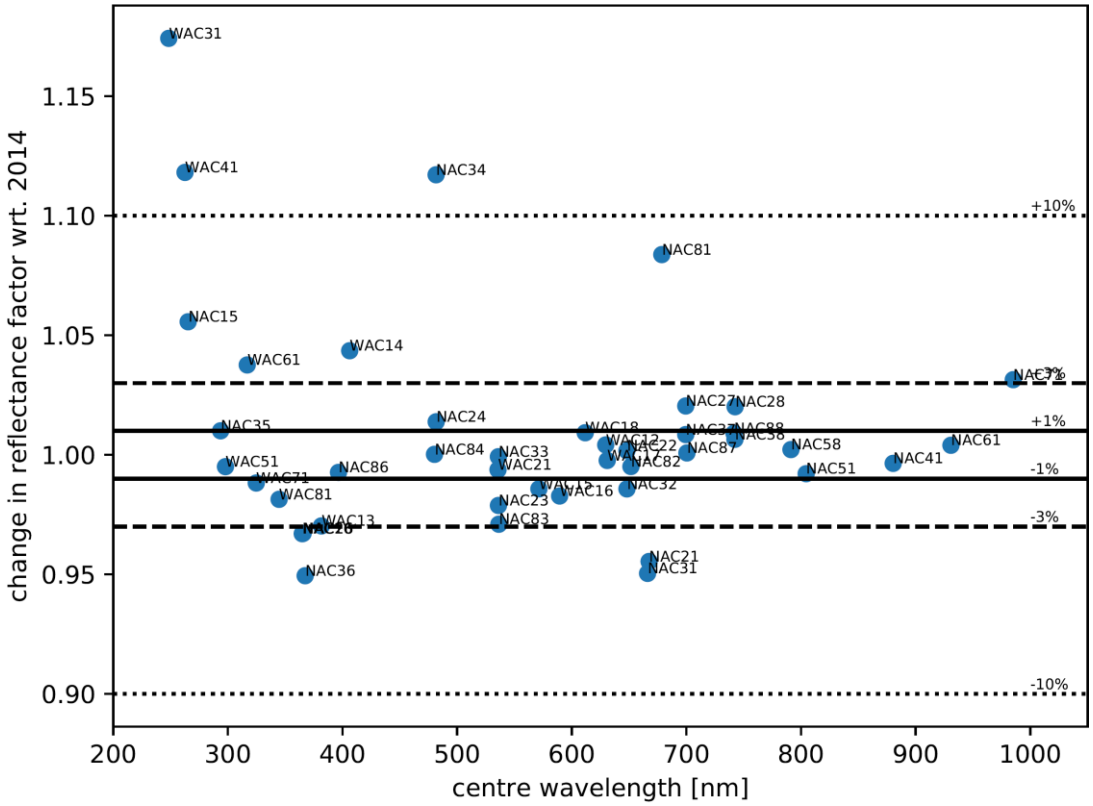

Figure 2: Reflectance factor per filter compared to factors from 2014 (version 1/b of this document).

2.4 Validation

As a means of validation and cross check, the aperture photometry from 16 Cyg was compared against the spectral irradiance of a solar spectrum scaled to the 16 Cyg V magnitude. All filters show a good match with the 16 Cyg spectrum. For 2014 factors, the four filters mentioned above had a clear mismatch but are matching the curve with the new calibration factors. It should be noted that filters 21, 31, and 81 are derived from the 16 Cyg spectrum and fit by definition (their offset with respect to the spectral curve is not a contradiction but due to the very broad band integration of these filer combinations). WAC filters were not used in this study as the aperture photometry optimised for Vega (bright star compared to background, working with large aperture region) results in larger errors for 16 Cyg without extra effort in adaption of the algorithm.

A further comparison was drawn to the reflectance of asteroid 4 Vesta, following the work of Fornasier et al. (2011, A&A 533:L9). This is presented in Figure 4, where the solid green line denotes the visible Vesta spectrum as scaled by Fornasier et al. The black crosses are the data points by Fornasier and converted to the new reflectance factors. The dashed black line is the same spectrum but linearly scaled to optimise the deviation to the black crosses. This shows a systematic offset and resulting smaller albedo using the new reflectance factors. The blue and orange symbols are our aperture photometry measurements of Vesta, which show a similar deviations with respect to the blue curve that was fitted to this data. Reflectance factors from 2014 show a slightly better but comparable χ^2 (7.3 or $9.1 \cdot 10^{-4}$ depending on whether we use the aperture photometry from Fornasier et al. or our photometry).

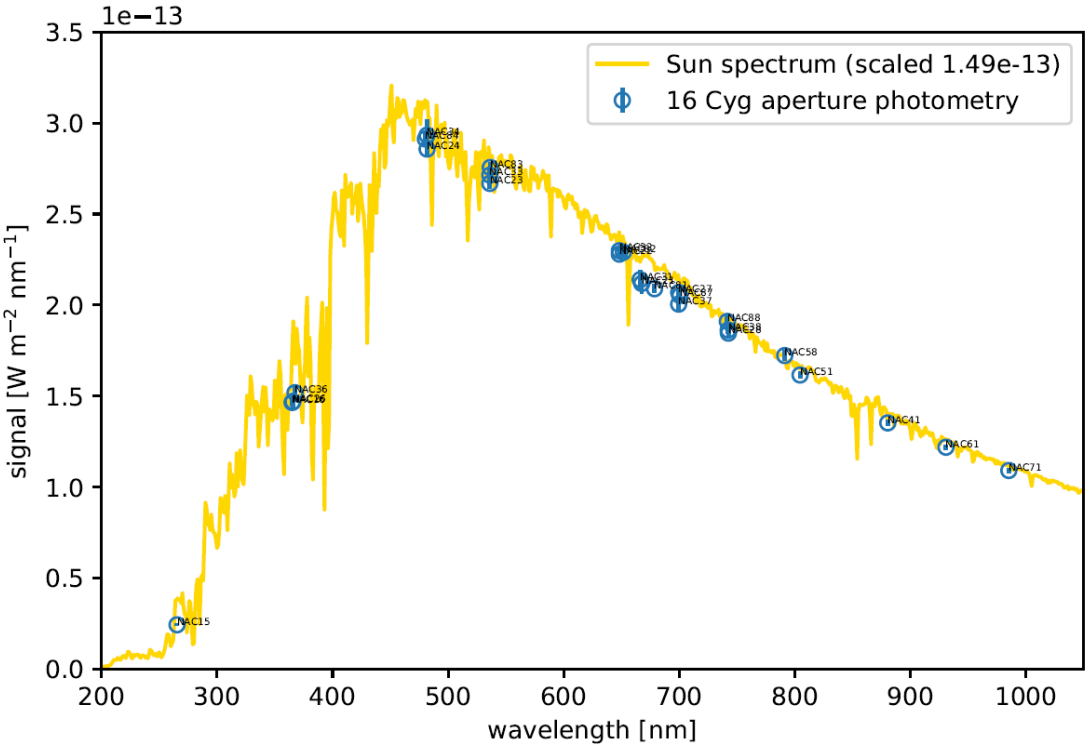

Figure 3: Spectral irradiance of 16 Cyg determined from aperture photometry in comparison to scaled solar spectrum.

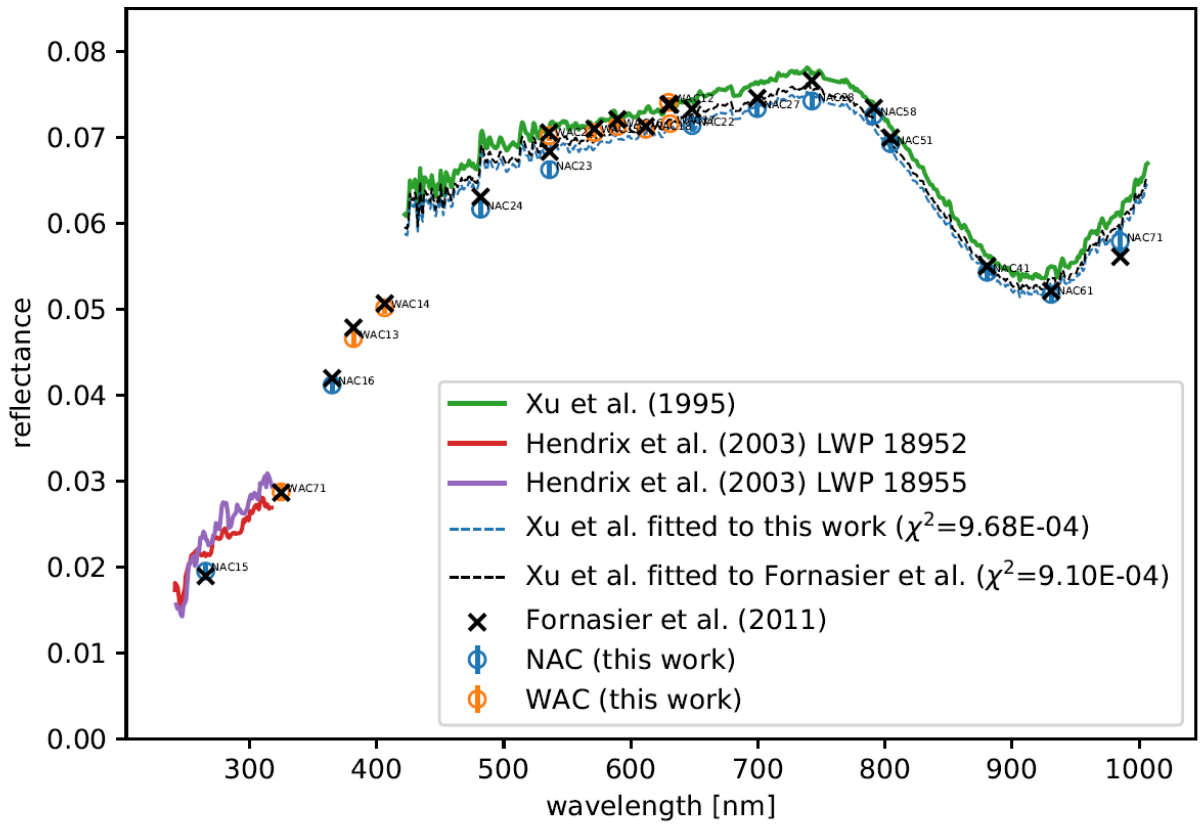

Figure 4: Reflectance of 4 Vesta compared to OSIRIS photometry with new reflectance factors

3 Camera Throughput and Spectra of Stars

3.1.1 Instrument Throughput

For the instrument sensitivity, we require spectral transmission of filter elements and ARP, spectral reflectance of the mirrors and the quantum efficiency.

3.1.1.1 Filters

Filter transmission curves are presented in [RD10].

3.1.1.2 Mirrors

NAC and WAC are a 3-mirrors and 2-mirrors off-axis system, respectively [RD1]. The total reflectivity of the mirror system is the single-mirror reflectance to the power of the number of mirrors.

The measurement of the WAC mirror reflectivity is reported in [RD5].

3.1.1.3 Anti-Radiation Plate (ARP)

Both cameras are equipped with an Anti-Radiation Plate (ARP), installed directly in front of the CCD, for radiation shielding [RD1]. The measured transmissivity of the WAC APR is reported in [RD4].

Re-measurement of the transmissions of the two GRM ARPs at PTB Braunschweig in August 2021 showed slight differences in transmission in the order of 2% but little consequence to the absolute calibration factors. The effect on these would be 0.1%, so it was decided to keep the data from the measurements on the flight units.

The total reflectivity of the mirrors and the transmissivity of the ARPs are shown in Figure 5.

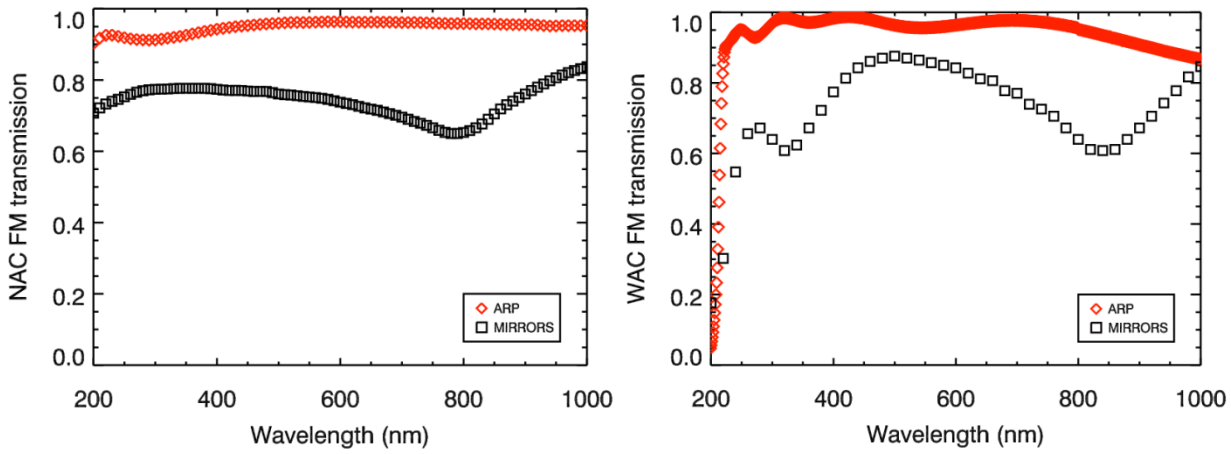

Figure 5: Measured total reflectivity of the mirrors and transmissivity of the ARPs for NAC (left) and WAC (right).

3.1.1.4 Quantum Efficiency

OSIRIS NAC and WAC are equipped with (by design) identical CCDs, that are coated using "mid-band coating" [RD1]. The quantum efficiency by design of the CCDs is shown in Figure 6.

During the ground calibration, the quantum efficiency of the NAC [RD3] and WAC [RD2] CCDs (with IDs 243 for NAC and 242 for WAC) were measured on the flight models at room temperature

(295 K) and close to operational temperature (180 K). The measured QEs are tabulated in Table 4 and shown in Figure 7.

For the throughput integration we use the quantum efficiency per camera, measured at 180 K.

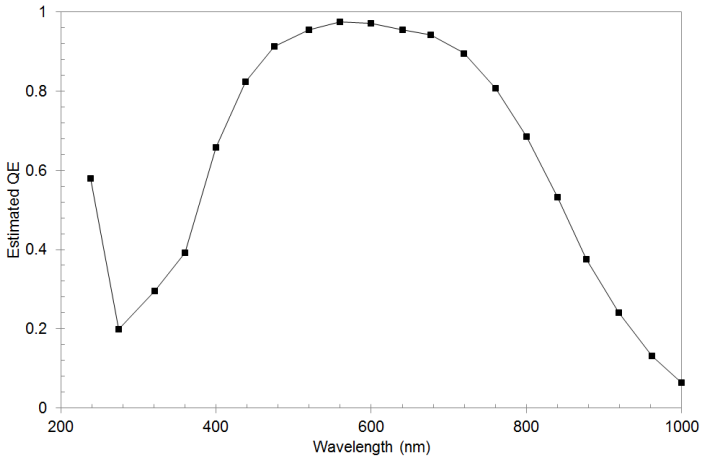

Figure 6: Quantum efficiency by design of the OSIRIS CCDs.

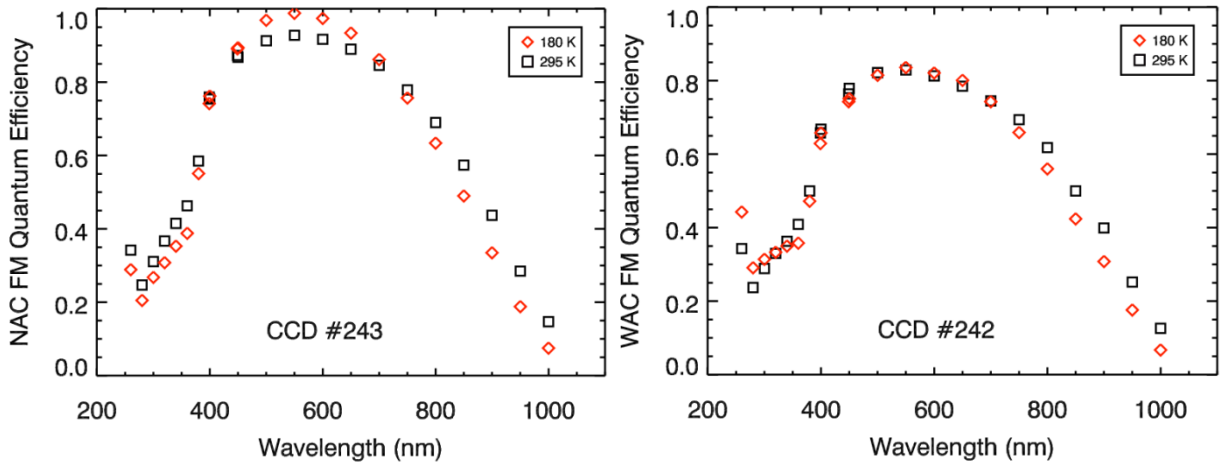

Figure 7: Quantum efficiency of the NAC (left) and of the WAC (right) CCD, as measured on the flight models at room temperature (295 K) and close to operational temperature (180 K).

Table 4: Quantum efficiency of the NAC and of the WAC CCD, as measured on the flight models at room temperature (295 K) and close to operational temperature (180 K).

Wavelength [nm]	NAC CCD #243		WAC CCD #242	
	QE @ 295 K	QE @ 180 K	QE @ 295 K	QE @ 180 K
260	0.342	0.289	0.343	0.443
280	0.247	0.205	0.237	0.291
300	0.311	0.268	0.289	0.314
320	0.367	0.308	0.33	0.333
340	0.415	0.353	0.363	0.35
360	0.463	0.388	0.409	0.358
380	0.585	0.551	0.5	0.472
399	0.759	0.742	0.658	0.629
400	0.754	0.762	0.668	0.658
449	0.873	0.891	0.764	0.743
450	0.868	0.894	0.779	0.751
500	0.913	0.969	0.822	0.815
550	0.928	0.988	0.829	0.836
600	0.917	0.974	0.813	0.821
650	0.89	0.934	0.785	0.801
700	0.846	0.862	0.745	0.743
750	0.779	0.757	0.694	0.659
800	0.69	0.634	0.618	0.56
850	0.574	0.49	0.5	0.424
900	0.437	0.335	0.399	0.308
950	0.285	0.188	0.252	0.176
1000	0.147	0.075	0.126	0.067

3.1.2 Spectral Irradiance of Sun and Calibration Stars

For the Vega spectrum we use a spectrum provided in the CALSPEC database from the Space Telescope Science Institute. Earlier versions of the OSIRIS calibration factors were based on version 005 of this spectrum and we updated to the latest version 010 with a much improved uncertainty of 1%.

For the solar spectrum, we compared spectra of Colina et al. (1996, AJ 112:1)[1] which was used for OSIRIS calibration until earlier versions of this document (before 2/-) with spectra from Thuillier et al. (2004, Geoph. Mono. 141, AGU, p. 171), Woods et al. (2009, GRL 36:L01101), and Meftah et al. (2018, A&A 611:A1). The advantage of the latter three is that they provide a total solar irradiance (TSI), which is the integral of these spectra plus a modelled energy outside the measured bands. This can be compared to the TSI of $1360.8\,\mathrm{W\,m^{-2}}$ recommended by the IAU.

We decided to use the spectrum by Thuillier et al. and scaled it from a TSI of $1382.74\,\mathrm{W\,m^{-2}}$ to $1360.8\,\mathrm{W\,m^{-2}}$. This spectrum is also recommended on the CALSPEC database, the file was provided upon request by G. Thuillier. The uncertainty is provided as 2 to 4 % in the paper. A comparison of the four spectra showed a typical spectral uncertainty in the order of 2.5 % when folded with the OSIRIS band passes, which we use as an error.

[1] The spectrum is compiled by Colina et al. and based on measurements of Woods et al. (1996, JGR 110:D6) for 119.5 to 410 nm, Neckel & Labs (1984, Sol Phys. 90:205) for 410 to 870 nm, Arvesen et al. (1969, Appl. Opt. 8:11) for 870 to 960 nm and a model by Colina et al. beyond 960 nm.

For the spectrum of 16 Cyg A&B (incl. 16 Cyg C), we use our solar spectrum and scale it according to the V magnitude of 16 Cyg A&B combined and the Sun, assuming $m_{\mathrm{Sun}} = -26.75$ and $m_{16\mathrm{Cyg}} = 5.315$, which results in a scaling factor of $1.49 \cdot 10^{-13}$.

Table 5: Spectral energy distributions.

Star	**SED**
Vega	alpha_lyr_stis_010.fits
Sun	ATLAS3 RESAM-1 nm 0-2397.txt (Thuillier et al. 2004; scaled to IAU TSI)
16 Cyg A&B	Sun spectrum scaled to V magnitude of 16 Cyg A&B (factor $1.49 \cdot 10^{-13}$)

4 Calibration files used by OsiCalliope

The calibration files used by OsiCalliope to calibrate OSIRIS images are:

- NAC_FM_ABSCAL_V02.TXT (since version 2/- of this document)
- WAC_FM_ABSCAL_V02.TXT (since version 2/- of this document)

The data files used to determine the throughput of the cameras are (stored in OsiCalliope THROUGHPUT folder):

- Quantum efficiency:
  - NAC_FM_QE_V01.TXT
  - WAC_FM_QE_V01.TXT
- Reflectivity of the mirrors:
  - NAC_FM_MIRROR_V01.TXT
  - WAC_FM_ MIRROR _V01.TXT
- Transmissivity of the ARPs:
  - NAC_FM_ARP_V01.TXT
  - WAC_FM_ ARP _V01.TXT

Previous versions:

- NAC_FM_ABSCAL_V01.TXT (until version 1/b of this document)
- WAC_FM_ABSCAL_V01.TXT (until version 1/b of this document)
- NAC_FM_ABSCAL_FACTORS.LBL (same values as NAC_FM_ABSCAL _V01.TXT)
- WAC_FM_ABSCAL_FACTORS.LBL (same values as WAC_FM_ABSCAL_V01.TXT)